Software-Defined Virtual Synchronous Condenser

Jiang, Zimin; Zhang, Peng; Zhou, Yifan; Kocewiak, Lukasz; Chandrashekhara, Divya Kurthakoti; Picherit, Marie-Lou; Tang, Zefan; Bowes, Kenneth B.; Yang, Guangya

Published in:
IEEE Transactions on Power Systems

Link to article, DOI:
10.1109/TPWRS.2024.3444701

Publication date:
2025

Document Version
Peer reviewed version

Software-Defined Virtual Synchronous Condenser

Zimin Jiang, *Graduate Student Member, IEEE,* Peng Zhang, Yifan Zhou, *Member, IEEE,* Lukasz Kocewiak, *Senior Member, IEEE,* Divya Kurthakoti Chandrashekhara, Marie-Lou Picherit, Zefan Tang, *Member, IEEE,* Kenneth B. Bowes, and Guangya Yang, *Senior Member, IEEE*

***Abstract*—Synchronous condensers (SCs) play important roles in integrating wind energy into relatively weak power grids. However, the design of SCs usually depends on specific application requirements and may not be adaptive enough to the frequently-changing grid conditions caused by the transition from conventional to renewable power generation. This paper devises a software-defined virtual synchronous condenser (SDViSC) method to address the challenges. Our contributions are fourfold: 1) design of a virtual synchronous condenser (ViSC) to enable full converter wind turbines to provide built-in SC functionalities; 2) engineering SDViSCs to transfer hardware-based ViSC controllers into software services, where a Tustin transformation-based software-defined control algorithm guarantees accurate tracking of fast dynamics under limited communication bandwidth; 3) a software-defined networking-enhanced SDViSC communication scheme to allow enhanced communication reliability and reduced communication bandwidth occupation; and 4) Prototype of SDViSC on our real-time, cyber-in-the-loop digital twin of large-wind-farm in an RTDS environment. Extensive test results validate the excellent performance of SDViSC to support reliable and resilient operations of wind farms under various physical and cyber conditions.**

***Index Terms*—Wind farms, virtual synchronous condenser, software-defined control, software-defined networking**

I. Introduction

OFFSHORE wind energy has been increasingly integrated into power grids. For instance, the State of New York has set the goal of integrating 9 GW offshore wind by 2035 to help build 100% electricity grids powered by zero-emission resources [1]–[3]. Large scale integration of offshore wind energy poses challenges to the operation of weakened power grid [4]–[6].

One effective approach to support large-scale integration of offshore wind energy is to use synchronous condensers (SCs), which can provide inertia [7], frequency regulation support [8], short-circuit current contribution [9], and sub/super-synchronous oscillations suppression [10] to the grid. However, conventional SCs are synchronous machines and their designs (e.g., locations and capacities) highly depend on the application scenarios [11], [12]. Correspondingly, the deployment and upgrade of SCs are highly expensive and they are unable to adapt to the frequently changing grid conditions [9]. Virtual synchronous generators (VSGs) has been proposed to emulate synchronous machine behaviors with inverter-based resources [13]–[15], whereas it offers limited capability to provide fast voltage/reactive power support for the system, especially under grid fault conditions.

The overarching goal of this paper is to originate a lightweight, cost-effective, and adaptive approach to achieve the SC functionalities for wind energy integration. Whereas, at the wind turbine and wind farm level, inverter controllers can provide built-in capabilities to realize various control functionalities, such as hierarchical control, synthetic inertia and instability damping [16]. Intuitively, if the inverter controllers are properly designed, they will be able to provide the desired SC functionalities while avoiding deploying the real synchronous machine hardware. On the other hand, software-defined control (SDC) [17], a recently emerging technology, also provides insights into resolving the hardware dependence issue. SDC virtualizes traditionally hardware-dependent inverter controllers into software-defined services and, in this way, realizes ultra-flexible and cost-effective controllers for power grids with significantly enhanced programmability and deployability.

In summary, this paper develops a software-defined virtual synchronous condenser (SDViSC), which realizes the SC functions without requiring the deployment of real SCs and hardware-dependent controllers. The main contributions are:

- **Architecture of virtual synchronous condenser (ViSC)**: We enable a built-in capability of wind turbines to provide programmable SC functions such as flexible Var capability, inertia, oscillation damping, and weak grid enhancement.
- **Engineering SDViSC**: We accomplish SDViSC by devising a Tustin transformation-based SDC algorithm to virtualize the hardware ViSC controller as a software service, which enables capturing the fast dynamics of ViSC under limited communication bandwidth.
- **Resilient SDViSC communication by SDN**: We further establish software-defined networking (SDN)-enabled communication for SDViSC to enable reliable operations of SDViSCs with low delays and high robustness even under communication network impairments.
- **Validated Prototype of SDViSC**: A cyber-in-the-loop large-wind-farm prototype with 50 wind turbines is built in an RTDS environment, and extensive test results validate the superior programmability and flexibility of SDViSC and its capability to enable reliable operations of wind farms under weak grid conditions and cyber failures.

The remainder of this paper is organized as follows. Section II presents the design of ViSC and SDViSC. Section III

This paper is based upon work supported by the U.S. Department of Energy's Office of Energy Efficiency and Renewable Energy (EERE) under the Solar Energy Technologies Office Award Number DE-EE0009341.

Z. Jiang, P. Zhang, Y. Zhou and Z. Tang are with the Department of Electrical and Computer Engineering, Stony Brook University, Stony Brook, NY 11794, USA. (e-mail: p.zhang@stonybrook.edu).

L. Kocewiak, D. K. Chandrashekhara and M.-L. Picherit are with Ørsted Wind Power, 7000 Fredericia, Denmark.

K. B. Bowes is with Eversource Energy, Berlin, CT 06037, USA.

G. Yang is with the Center for the Electric Power and Energy, Technical University of Denmark, 2800 Lyngby, Denmark.

develops the SDN-enhanced SDViSC. Section IV presents the established digital twin of SDViSC and provides extensive experiments to validate the performance of SDViSC. Section V concludes the paper.

II. SDViSC for Wind Energy Integration

This section devises SDViSC, a software-defined virtual synchronous condenser, as seen Fig. 1, to support wind energy integration in an unprecedentedly programmable, adaptative and lightweight manner. In this paper, ViSC refers to SC functionalities provided by inverters with controllers implemented on specific hardware, such as DSP or PLC; SDViSC means that SC functionalities are provided by inverters with pure software-based controllers.

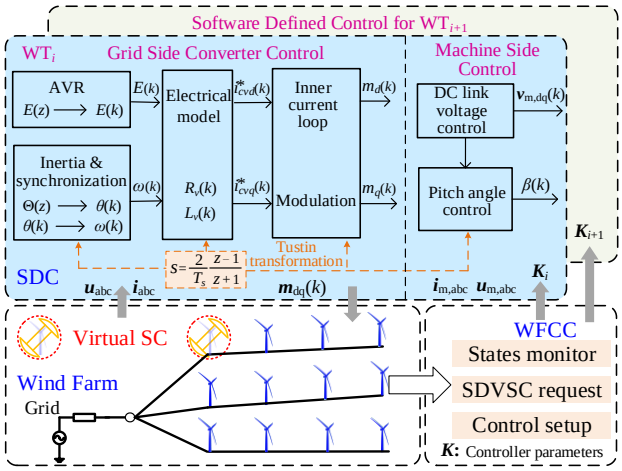

Fig. 1. Design overview of SDViSC.

A. Architecture of ViSC

We first design ViSC for an individual wind turbine to achieve the following control functions of SCs: i) to provide a natural inertial response and a short-circuit current, and ii) to generate or absorb reactive power to support voltage regulation. The design of ViSC includes control strategies for both grid-side and machine-side converters.

1) Grid-Side Control: Our design of the grid-side converter adopts a double-loop control, as shown in Fig. 2. The outer-loop control is designed to achieve the following functionalities (see Fig. 2(a)): i) a mechanical model to provide inertia emulation and synchronization with the grid; ii) a voltage controller to provide the automatic voltage regulation (AVR) as conventional SCs, where an electrical model represents the stator windings; and iii) a supplementary controller customized to provide auxiliary control functions.

For the inertia emulation part, the transfer function to generate the phase angle δ is formulated as:

$$\Theta(s) = \frac{1}{2Hs^2 + Ds} T(s) + \frac{1}{s} W(s) \tag{1}$$

where $\Theta(s)$, $T(s)$ and $W(s)$ are the Laplace transforms of the phase angle δ, injected torque error T_{err}=T_m-T_e ($T_m = 0$ due to no input mechanical power), and the reference angular

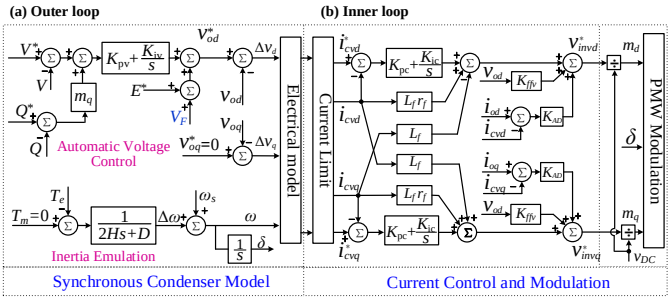

Fig. 2. Grid-side control of ViSC.

frequency ω_s, respectively; H and D are the emulated inertia constant and the damping factor of the ViSC, respectively.

For the AVR part, its transfer function is formulated as:

$$E = [(V^* - V) + m_q(Q^* - Q)](K_{pv} + \frac{K_{iv}}{s}) + E^* + V_F \tag{2}$$

where K_{pv} and K_{iv} are the PI parameters of AVR; and m_q is the droop coefficient; E, V, Q, E^*, V^* and Q^* are the AVR output, output voltage, output reactive power and the corresponding references, respectively; V_F is the output of the supplementary controller, which will be discussed in (4).

The internally-induced voltage of the AVR block (i.e., E) is further connected with an electrical module to represent the electrical behavior of a synchronous machine. A commonly-adopted quasi-stationary electrical model is applied [18]:

$$\tilde{i}_{cvd} + j\tilde{i}_{cvq} = \frac{E - (v_d + jv_q)}{R_v + jX_v} \tag{3}$$

where $R_v = R_{vir}/[(\omega L_{vir}/\omega_s)^2 + R_{vir}^2]$ and $X_v = (\omega L_{vir}/\omega_s)/[(\omega L_{vir}/\omega_s)^2 + R_{vir}^2]$ represent the dynamic impedance; R_{vir} and L_{vir} are the virtual resistance and inductance; ω is the angular frequency of ViSC. v_d and v_q denote the output voltage measured locally under the dq-coordinates. A circular current limiter [19] is applied to limit the amplitude and preserve the angle of the output of the electrical model $\tilde{i}_{cvd} + j\tilde{i}_{cvq}$. The output of the current limiter, i.e., $i^*_{cvd} + ji^*_{cvq}$, provides the current reference for the inner-loop controller.

For the supplementary control block, in this paper, we design the following virtual friction control function to help ViSC suppress power oscillations and improve the frequency stability under weak grid conditions:

$$V_F(s) = \frac{W(s) - \Omega(s)}{1 + sT_{LPF}} \left(\frac{K_{F1}s}{1 + sT_{v1}} + \frac{K_{F2}s}{1 + sT_{v2}}\right)\left(\frac{1 + sT_1}{1 + sT_2}\right)^2 \tag{4}$$

where T_{LPF}, T_{V1}, T_{V2}, T_1 T_2 and K_{F1}, K_{F2} are the controller's time constants and gains; the input signal is the frequency deviation $(\omega_s - \omega)$, $\Omega(s)$ is the Laplace transform of ω; the output signal V_F is then sent to the AVR block as shown in (2). Eq. (4) adopts two control signals, i.e., the frequency deviation and the rate of change of frequency, to damp the power oscillation. A lead-lag controller to adjust the output magnitude is also used to further help oscillation suppression due to its better trade-off between static accuracy and stability.

The inner loop of the grid-side converter, as detailed in Fig. 2(b), includes a decoupled PI controller, a voltage feed-forward controller and an additional active damping controller,

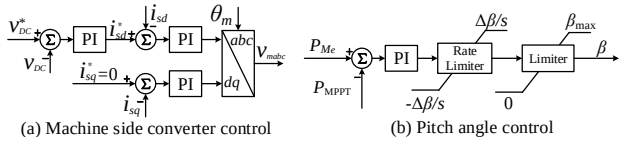

(a) Machine side converter control (b) Pitch angle control

Fig. 3. Machine-side control.

which improves the output current quality and suppresses filter voltage oscillations.

2) Machine-Side Control: As for the machine-side control, our main target is to maintain a constant DC link voltage regardless of variations in the wind turbine machine speed ω_r and torque. This is achieved by the machine-side converter control and the pitch angle control, as shown in Fig. 3.

For the machine-side converter control (see Fig. 3(a)), the DC link voltage difference $(v^*_{DC} - v_{DC})$ is regulated by a PI controller to generate the stator d-axis current reference i^*_{sd}. The stator q-axis current reference i^*_{sq} is set as 0, because the active power P_{Me} generated by the machine can be expressed as $P_{Me} = \frac{2}{3}\psi\omega_r i_{sq}$ [20], where ψ is the stator magnetic flux linkage. The pitch angle control (see Fig. 3(b)) is used to match the power P_{Me} consumed by the machine to maintain constant DC link voltage. The difference between P_{Me} and the captured wind power P_{MPPT} using maximum power point tracking (MPPT) is sent to a PI controller and the reference pitch angle is obtained through the pitch angle control framework [21].

The parameters of all designed controllers are provided in the Appendix.

Consequently, through ViSC, wind turbines can provide inertia support and voltage regulation as conventional SCs. Moreover, it provides programmable control performance to some extent, because the inertia constant and damping factor in corresponding control blocks can be flexibly adjusted.

B. SDViSC: Software-Defined ViSC

Further, we discuss how to engineer an SDViSC, i.e., realizing ViSC in edge computing to fully release the virtualization and programmability advantages. The key to the development is a Tustin transformation-based SDC approach.

The basic philosophy of SDC is to achieve hardware-dependent control functions in a software manner by discretizing all continuous-time controllers into discrete-time ones [17]. During the SDC discretization procedure, conventional numerical integrators, such as Euler and trapezoidal methods, usually require small sampling rates to track fast dynamics to perform real-time control [17], [22], which unavoidably increases communication burdens from the SDC unit to WTs (see Section III), e.g., large communication bandwidth consumption.

To bridge the gap, this subsection devises a control-loop (outer loop and inner loop) based SDC algorithm to realize SDViSC under fast dynamics and limited communication bandwidth. It guarantees the performance of SDViSC under real-time applications by balancing the output accuracy and computation speed.

1) Tustin Transformation: The Tustin transformation is essentially a Taylor expansion-based "s to z" mapping of z=e^{sT_s}, as shown below:

$$s = \frac{1}{T_s} Ln(z) = \frac{2}{T_s} \sum_{k=1}^{\infty} \frac{1}{2k-1} \left(\frac{z-1}{z+1}\right)^{2k-1} \tag{5}$$

where T_s is the sampling period. Using only the first term, the Tustin transformation is defined as follows:

$$s = \frac{2}{T_s} \frac{z-1}{z+1} \tag{6}$$

The Tustin transformation preserves the properties of stability and the minimum phase of the original continuous-time controllers [23]. Thus, the original controllers' performance can be guaranteed after discretization without requiring tiny sampling rates as required by conventional integration rules [17].

Next, we discretize ViSC using the Tustin transformation.

2) Discretization of the AVR Block: PI controllers are the main-body of the AVR block. Given an arbitrary PI controller with the input $e_r(t)$, output $g(t)$ and parameters K_p and K_i, the Tustin transformation can be performed as:

$$G(z)(1-z^{-1}) = [\frac{T_s}{2} K_i (1+z^{-1}) + K_p (1-z^{-1})] E_r(z) \tag{7}$$

where $G(z)$ and $E_r(z)$ are the z transforms of $g(t)$ and $e_r(t)$. The PI controller output can be calculated recursively as:

$$\begin{aligned} g(k) = g(k-1) + \frac{T_s}{2} K_i (e_r(k) + e_r(k-1)) + K_p (e_r(k) \\ - e_r(k-1)) \end{aligned} \tag{8}$$

Consequently, the output voltage E of the AVR controller is calculated by the following rule:

$$\begin{aligned} E(k) = E(k-1) + \frac{T_s}{2} K_{iv} [2(V^* + m_q Q^*) - V(k-1) \\ - V(k) - m_q (Q(k) + Q(k-1))] - K_{pv} (V(k) \\ - V(k+1) - m_q (Q(k) - Q(k-1))) + V_F(k) \end{aligned} \tag{9}$$

Compared with SDC using conventional numerical integration rules, a notable feature of the Tustin transformation-based SDC is that (8) does not involve the cumulative control error. For example, the trapezoidal rule-based method [17] leads to a discretization of the PI controller as follows:

$$g(n) = K_p e_r(n) + T_s K_i \Big(\frac{e_r(0) + e_r(n)}{2} + \sum_{k=1}^{n-1} e_r(k) \Big) \tag{10}$$

For each time step, (10) needs to compute the cumulative control error ($\sum_{k=1}^{n-1} e_r(k)$), whereas (8) has no such requirements.

As a result, the devised Tustin transformation-based SDC can ensure that the control performance is unaffected by historical errors and therefore provides improved numerical stability. In other words, the Tustin transformation-based SDC can eliminate the steady-state error even using moderate sampling rates, which significantly reduces the communication burden.

3) Discretization of the Inertia Emulation Block: This subsection derives the discretization rule of the outputs (i.e., phase angle δ and angular frequency ω) of the inertia emulation block. Substituting (6) into (1) yields the following:

$$\Theta(z) = \Big[\frac{1}{2H(\frac{2}{T_s}\frac{z-1}{z+1})^2 + D\frac{2}{T_s}\frac{z-1}{z+1}} \Big] T(z) + \frac{1}{\frac{2}{T_s}\frac{z-1}{z+1}} W(z) \tag{11}$$

where $\Theta(z)$ denotes the z transform of δ. Normalize the constant term in the denominator of the transfer function in (11) to 1, and after rearrangement and let $K = 2/T_s$, we have:

$$\Theta(z) = (1 - \frac{4HK^2}{2HK^2+DK}z^{-1} + \frac{2HK^2-DK}{2HK^2+DK}z^{-2}) + \frac{T(z)}{2HK^2+DK}(1+2z^{-1}+z^{-2}) + \frac{W(z)}{K}(1-z^{-2}) \tag{12}$$

Consequently, the discretized recursive equation of $\delta(n)$ is

$$\delta(k) = \frac{4HK^2}{2HK^2+DK}\delta(k-1) - \frac{2HK^2-DK}{2HK^2+DK}\delta(k-2) + \frac{1}{2HK^2+DK}\Big[T_e(k) + 2T_e(k-1) + T_e(k-2)\Big] + \frac{1}{K}\Big[\omega_s(k) - \omega_s(k-2)\Big] \tag{13}$$

Then, ω can be readily obtained from the derivative of δ:

$$\omega(k) = [\delta(k) - \delta(k-1)]/T_s \tag{14}$$

Other control blocks, such as the inner-loop controller, supplementary controllers, can also be discretized using the same procedure to conduct the software-based implementation. Due to page limitations, details are omitted here. Finally, SDViSC is constructed by integrating all the discretized control blocks.

C. Programmable Management of SDViSCs for Wind Farm Operations

Up to this point, we have achieved SDViSC for an individual wind turbine. Further, in a wind farm, wind turbines equipped with SDViSC can operate in parallel to increase the available ViSC capacity. Although SDViSC can also be implemented locally using Internet of Things (IoT) devices, effective management of multiple SDViSCs supported by the SDC unit can better assist wind farm-level operations.

Because of the utilization of SDC, each wind turbine equipped with SDViSC can flexibly switch its operating mode between the ViSC mode and various grid-following/grid-forming modes (e.g., V/f control, P/Q control, droop control). The wind farm control center (WFCC) manages the software-defined operations of wind turbines:

- Once a wind turbine is required to operate at the ViSC mode, the WFCC sends out control commands to the SDC unit. The SDC unit, e.g., a physical server or a virtual machine, will allocate computing resources, and initialize the SDViSC for a specific wind turbine in the wind farm, which includes the operating mode switching command, the programmable parameters of the ViSC (e.g., emulated inertia and damping factor), and the supplementary control functions to be applied. The SDC unit can be conveniently placed in the WFCC or close to wind turbines (e.g., on the offshore platform).
- Then, the SDC unit runs the discretized controllers (detailed in Subsection II-B) based on local measurements at each sampling time and outputs the control signals (e.g., signals for generating SPWM and adjusting pitch angle) to the destination wind turbine to perform the ViSC control.
- Additionally, the SDC unit can also generate backup controllers operating in the "hot standby" mode to provide control redundancy and better robustness. The backup controllers will immediately pop up once there is a failure in the master controllers.

In summary, with SDViSC, the SC functionalities become one type of built-in service that wind turbines can provide. SDViSC enables two types of programmability that can not be achieved by hardware-based SCs or ViSCs: i) all the control parameters can be programmed much more efficiently than hardware-inverter-based ViSC benefiting from the full softwarization; ii) the overall capability for providing the ViSC functionalities can also be flexibly programmed by switching the operating modes of wind turbines via SDC. Such programmabilities, without restrictions of hardware dependence, make SDViSC very adaptive to changing operating conditions and cost-effective for deployment and upgrading.

III. SDN-Enhanced SDViSC Management for Large-Scale Wind Energy Integration

Since SDViSC management involves frequent communications between WFCC, wind turbines and the SDC unit, a dependable communication network is indispensable for guaranteeing the reliable operations of SDViSCs. This section establishes a software-defined networking (SDN)-enabled communication scheme for SDViSC management, which allows for ultra-reliable communication with low delays or congestion and hence supports reliable delivery of SDViSC control signals in large wind farms with hundreds or even thousands of wind turbines.

A. Communication Activities in SDViSC Management

In the SDViSC management procedure detailed in Subsection II-C, three major communication activities are involved:

- **Monitoring**: For each wind turbine, its connection status (i.e., connected or exited) and the operation mode (i.e., ViSC mode or other modes) are continuously monitored and sent to the WFCC for event detection and decision making.
- **Measurements**: Once the ViSC mode is enabled for a specific wind turbine, measurements of this wind turbine, including the three-phase output voltages and currents, are sent to the SDC unit to implement the SDViSC control.
- **SDC/WFCC commands**: The SDC unit sends out the control signals (e.g., the modulation signals) to specific wind turbines. The WFCC may also send control commands, such as voltage references, to adjust the operation of SDViSCs.

Traditional communication networks cannot fulfill SDViSCs' data transmission requirements (i.e., low latency and high reliability) because of insufficient visibility to support real-time network monitoring and imprompt reactions to dynamic network conditions (e.g., congestion and link failure). SDN offers new insights into developing ultra-resilient, scalable and automatically configurable communication by separating the control/data planes and exploiting network virtualization technologies [24]. It enables direct control and reliable communication through various functions, such as dynamic routing, traffic prioritization and fast failover, and allows deploying new applications at a faster rate [25].

Inspired by the SDN philosophy, we perform SDViSC communications through an SDN-based communication network.

B. SDN-Enhanced SDViSC Management

The three-layered SDN-enhanced SDViSC architecture is illustrated in Fig. 4: 1) a physical layer containing wind turbines in wind farms, 2) a cyber layer where the SDN controller manages the communication network for SDViSCs, and 3) an application layer for implementing SDViSC as well as other grid-forming/grid-following controllers.

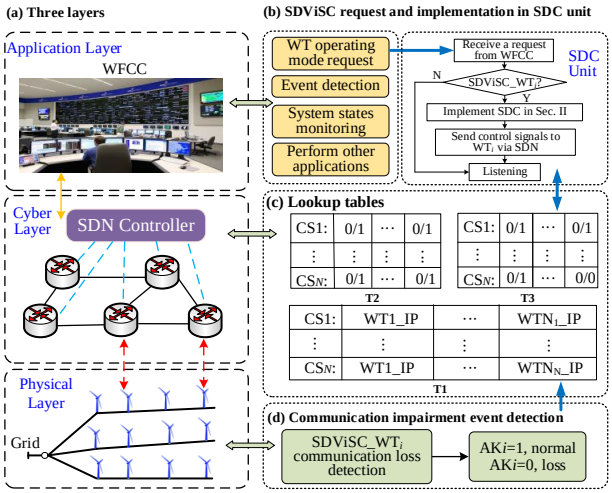

Fig. 4. SDN-enhanced SDViSC management.

1) Design of SDN Functions: According to the communication activities involved in SDViSC management, the SDN controller is designed to provide the following functions.

First, the SDN controller monitors the status of the cyber-physical system and dynamically updates the related information, including the connection status and operating modes of wind turbines, requests from WFCC, etc. Here, we design three lookup tables to store the monitored information (see details in Subsection III-B2): 1) the IP address table (T1), 2) the wind turbine's operating status and mode table (T2), and 3) the communication state table (T3). With those tables, the SDN controller can establish communication links as needed.

Second, the SDN controller manages the cyber system to ensure reliable and resilient communication to support SDViSC operations. For example, it can build communication links between the SDC unit and wind turbines as needed according to the information stored in T1, T2 and T3. It can also provide dynamic routing under network impairments, such as loss of communication. Here, we will design an event-based communication scheme to reduce communication burdens (see details in Subsection III-B3).

2) SDViSC Network Monitoring: Typically, a large wind farm is divided into clusters, each consists of a group of wind turbines connected in series. We use the cluster (CS) number and the wind turbine number for indexing to design the lookup tables to store the communication network information.

Using the IP protocol, each wind turbine has a unique IP address stored in T1 and retrieved by the SDN controller. T1 is updated when changes occur in the physical layer (e.g., plug-and-play of wind turbines) or in the communication configuration (e.g., adding, deleting, or modifying IP addresses).

T2 stores wind turbines' operating modes using three two-digit numbers for each wind turbine: '0/0', '0/1', and '1/1'. The first digit indicates the current operating mode, where '1' represents the ViSC mode and '0' are other modes. The second digit indicates whether the ViSC function is enabled, where '0' means disabled (i.e., the wind turbine cannot work in the ViSC mode) and '1' means enabled (i.e., the wind turbine can choose to work in the ViSC mode). Definitely, only when the ViSC mode is enabled, the current operating mode can be 1.

T3 stores wind turbines' communication states also using three two-digit numbers: '0/0', '0/1', and '1/1'. The first digit represents the current communication state between a wind turbine and the SDC unit, where '1' means the communication is on and '0' means off. The second digit indicates whether there exists a link satisfying the communication requirement, where '1' means yes and '0' means no.

3) Event-Based Communication for SDViSC Management: To reduce the communication bandwidth, we develop an event-based SDN communication scheme for SDViSC management so that communication is only required under specific events.

The following discusses two typical events: 1) SDViSC_WT$_i$, where the SDN controller receives a request to operate the i-th wind turbine in the SDViSC mode; 2) DR$_i$, where dynamic routing is required for the i-th wind turbine under communication impairments.

During wind farm operations, the SDN controller continuously listens to requests from WFCC. Once an SDViSC_WT$_i$ event is triggered, the SDN controller sends a command to the SDC unit and retrieves the IP address of the destination wind turbine from T1. Then, T2 and T3 are successively checked to confirm that the ViSC function is enabled and the corresponding communication state is on. Finally, the SDN controller creates flow tables for SDN switches to build communication links between the destination wind turbine and the SDC unit so that the SDViSC control can be readily performed.

Under communication impairments, the dynamic routing event DR$_i$ will be triggered to switch to a new communication path to guarantee reliable data transmission. Although the SDN controller provides a built-in function to periodically detect the network status, its performance is limited by the detection period and thus may not respond timely. Therefore, to ensure fast dynamic routing, we define an acknowledge signal AK$_i$ to detect the network performance. If the i-th wind turbine receives packets from the SDC unit normally, AK$_i$ is 1; otherwise, it changes to 0. Then, AK$_i$ is sent back to the SDN controller to check whether the dynamic routing should trigger by DR$_i$ = SDViSC_WT$_i$ $\wedge$ ($\neg$AK$_i$). A delay with $0.04s$ is added to the detection of DR$_i$ based on the delay effect analysis in [17]. The added delay ensures that false detection will not be induced because the communication delay of Ethernet switches is much smaller.

In summary, the SDN-enhanced SDViSC management offers three benefits unattainable by traditional communication techniques: 1) it can effectively manage the network configurations for all the wind turbines in the wind farm and perform dynamic routing under communication failures, which enables great flexibility, reliability and resilience for the communication between SDViSCs, the WFCC and the SDC unit; 2) it adopts an event-based scheme for the automatic

implementation of SDViSCs, including control signal generation, communication link building and control signal delivery, which avoids occupation of controller-to-switch bandwidth and reduces unnecessary data transmission; and 3) SDN benefits communications in complex networks by breaking communication barriers arising from proprietary protocols. This is because SDN directly controls the flow of data packets by creating the flow tables for routers among subnetworks, and adjusts data priority and throughput to avoid congestion. As such, SDViSCs' deployment and management are not constrained by specific communication infrastructures and protocols.

IV. Experimental Results

In this section, we thoroughly evaluate SDViSC's performance on a real-time and hardware-in-loop prototype using RTDS. First, we validate the Tustin transformation-based SDC algorithm. Second, the performance of the SDViSC in comparison to the traditional SC is presented. Third, we validate the control efficacy of SDViSC to support reliable and resilient operations of wind farms under various conditions. Last, we demonstrate the reliability and benefits of the SDN-enhanced communication scheme for SDViSC management.

A. Testing Environment Setup

1) Test System: Fig. 5 shows our designed 500 MW offshore wind farm (OWF) test system with 50 PMSG based wind turbines[1] to verify SDViSC. The 50 wind turbines are grouped into 5 clusters and integrated into the onshore power grid through a high-voltage alternating current (HVAC) cable. For comparison studies, a 40 MVAR traditional SC (referred to [7]) and an SDViSC with the same capacity by aggregating four wind turbines [16] are connected to the onshore point of coupling separately. Detailed designs are as follows:

- **Wind turbine controller**: Wind turbines originally adopt a grid-following-based double loop control. Detailed control topology and controller parameters are provided in [16].
- **Onshore grid**: It is modeled as an ideal voltage source connecting an impedance $R/X = 0.1$ in series. The short-circuit ratio (SCR) can be adjusted to emulate different grid conditions [16] to provide a thorough evaluation of SDViSC.

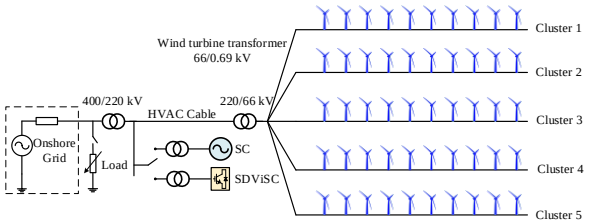

Fig. 5. Topology of the test system: a 500MW OWF with 50 wind turbines.

[1]The designed OWF is extended from the CIGRE C4.49 benchmark system, which has two equivalent wind turbines with aggregated models [16].

2) Real-Time Prototype: As depicted in Fig. 6, the SDViSC prototype has an OWF control center (OWFCC), an SDC unit, an SDN controller, four SDN switches, a traditional switch (L2 switch), GTNET×2 cards, RTDS hardware, and the power system simulation software RSCAD that interacts with the RTDS hardware. Detailed settings are as follows:

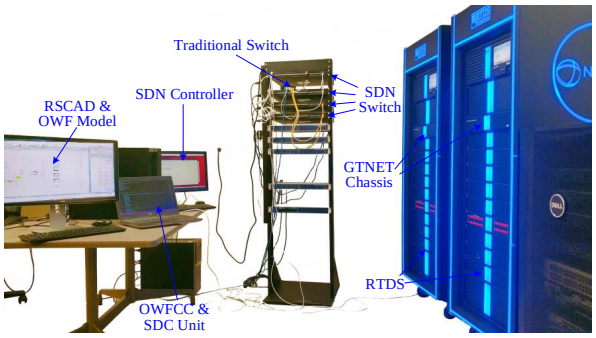

Fig. 6. Real-time, cyber-in-the-loop prototype for SDViSC.

- **Real-time OWF simulation**: The OWF system (see Fig. 5) is developed and compiled in RSCAD. Two RTDS racks with 10 cores are utilized to simulate the OWF in real time.
- **Communication setup**: GTNET×2 cards are utilized for RTDS hardware to communicate with external devices, such as the OWFCC and the SDC unit, over a LAN/WAN. The GTNET×2 cards provide Gigabit Ethernet ports for IP-based communications. UDP is used to transmit packets.
- **SDN setup**: A real SDN network with an SDN controller and four SDN switches running OpenFlow protocols are used to manage the communication network.

B. Numerical Stability of the Devised SDC Algorithm

This part verifies the numerical stability of our designed Tustin transformation-based SDC algorithm by comparing the performance of hardware-dependent ViSC and the SDViSC and demonstrates its superiority over the trapezoidal rule-based SDC algorithm [17]. ViSCs directly implemented in RSCAD emulate the performance of hardware-dependent controllers and serve as the ground truth for evaluating the performance of software-defined controllers. A phase-to-ground fault is studied, which occurs at the grid side at 1s and is cleared at 1.3s.

1) Performance Comparison between the ViSC and SDViSC: The solid lines in Fig. 7 illustrate the responses of hardware-dependent ViSCs. Fig. 7 (a) and (b) show that when the fault occurs, ViSCs immediately generate reactive power to support the grid voltage and successfully bring the system back to normal operation after the fault clearance. The phase angle θ in Fig. 7(c) from the inertial emulation block and the voltage reference in Fig. 7(d) for inner-loop modulation also demonstrate ViSCs function well as designed, i.e., providing inertia response and reactive power support as SCs do.

The dash lines in Fig. 7 illustrate the performance of SDViSC. A moderate sampling rate, i.e., 0.67ms, is adopted. As can be seen in the figure, the response curves overlap well and there is almost no obvious performance deterioration, which validates that SDViSC performs as well as the hardware-dependent ViSC. Therefore, our method can facilitate fast

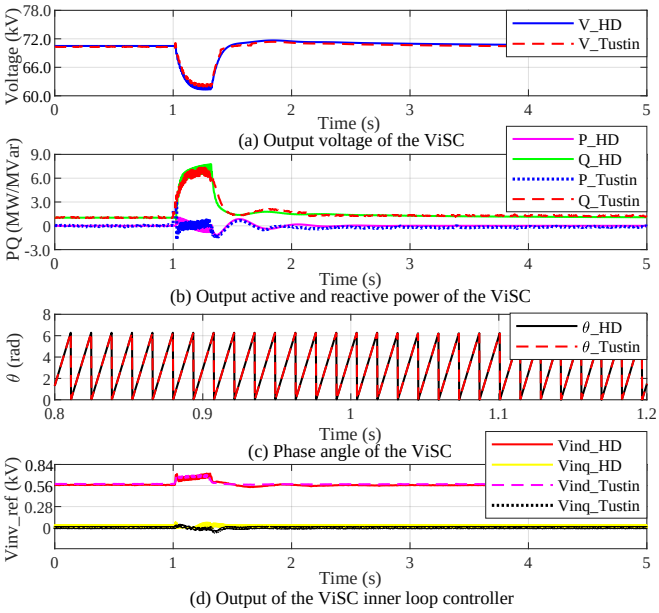

Fig. 7. Performance of ViSC using Tustin transformation-based SDC (sampling time: 0.67ms) and its comparison with hardware-dependent (HD) ViSC.

and low-cost deployment of SC functionalities with qualified control performance.

2) Performance of Tustin Transformation-based and Trapezoidal Rule-based SDC: In contrast, Fig. 8 presents the performance of the trapezoidal rule-based SDC algorithm [17] under a sampling rate 0.25 ms (i.e., the smallest sampling rate that can be realized under the communication bandwidth setting). It can be seen that the system collapses at around 2.2s, which indicates the trapezoidal-based SDC fails to provide the designed control functionality under limited communication bandwidth because of the accumulated historical error (as discussed in Subsection II-B2). Although further decreasing the sampling rate can improve the performance of trapezoidal-based SDC, it will unavoidably bring higher requirements on communication and increased vulnerability against network impairments.

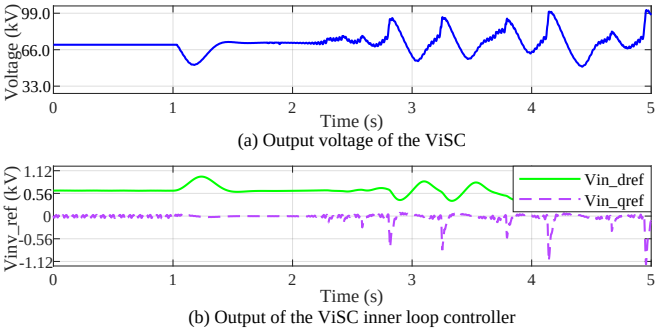

Fig. 8. Performance of trapezoidal rule-based SDC (sampling time: 0.25 ms).

As a conclusion, the Tustin transformation-based SDC ensures enhanced numerical stability compared over existing methods, evidenced by the fact that a much larger sampling rate (lower communication requirement) can be adopted without affecting the control performance.

C. Small-Signal Stability Analysis of SDViSC

Impedance-based stability analysis is widely used for small-signal stability analysis of inverter-dominated power systems. The impedance-scanning based method is adopted for the small-signal stability analysis of SDViSC. The system is divided at the point of common coupling (PCC) into two parts: the ViSC and the AC grid side, whose impedance responses $Z_{ac}(s)$ and $Z_{SC}(s)$ can be obtained by the frequency scanning method. The loop gain transfer matrix and its eigenvalues are given by $H_{cl}(s) = Z_{SC}(s)Z_{ac}^{-1}(s)$ and $\lambda_i(s) = eig[H_{cl}(s)]$ respectively [26], [27]. Generalized Nyquist stability Criterion (GNC) can be applied to determine the small signal stability as: If at least one of the eigenloci encircles the $(-1 + j0)$ (the phase angle curve crosses the -180 degree line) point in a clockwise manner as the frequency goes from -∞ to +∞, the system would be determined as unstable [26].

The impedance responses $Z_{ac}(s)$ and $Z_{SC}(s)$ obtained by the frequency scanning module in RTDS are presented in Fig. 9 and Fig. 10. The Bode plot of the eigenvalues is shown in Fig. 11. It can be seen from the results, there is no eigenloci encircles the $(-1 + j0)$ point in a clockwise manner as the frequency goes from -∞ to +∞. According to the GNC, the system is stable, which means the parameters of the system are well-tuned.

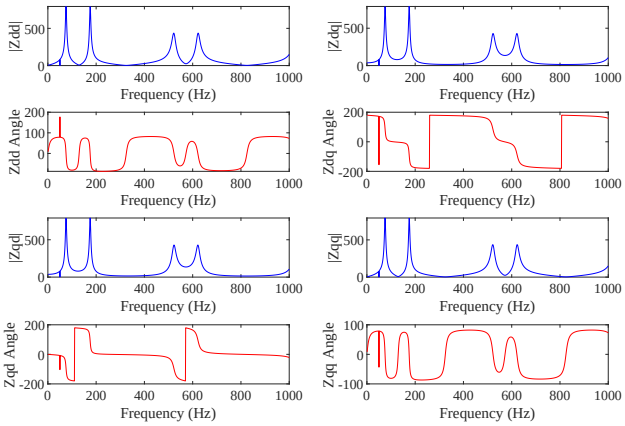

Fig. 9. Impedance results of the AC side system.

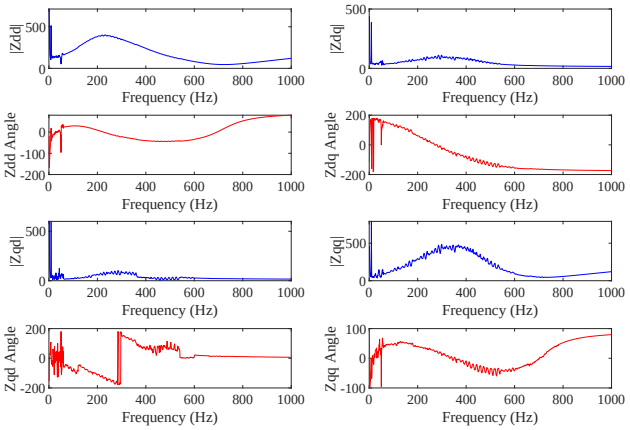

Fig. 10. Impedance results of the ViSC.

This article has been accepted for publication in IEEE Transactions on Power Systems. This is the author's version which has not been fully edited and content may change prior to final publication. Citation information: DOI 10.1109/TPWRS.2024.3444701

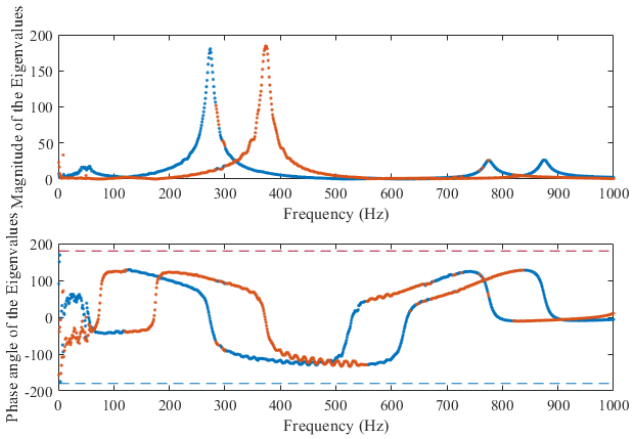

Fig. 11. Bode plot of the Eigenvalues.

D. Comparison between the SDViSC and Traditional SC

This subsection compares their performance from four aspects: voltage regulation capability, inertia support, short-circuit capacity contribution and grid strength enhancement.

1) Voltage Regulation Capability: Fig. 12 (a) presents the voltage regulation performance when changing the voltage references for the AVRs of the traditional SC and SDViSC from 66 kV to 69 kV at 1s separately. It can be seen that: 1) both the SC and SDViSC boost the voltage to around 68 kV finally; 2) SDViSC offers faster regulation speed and thus improved voltage regulation capability than the traditional SC.

Fig. 12 (b) shows the SDViSC's voltage stiffness characteristics, the inner potential's ability to tolerate the difference between the real and reference reactive power over a time interval. It is determined by $T_v = 1/K_{iv}$, the reciprocal of the integrator parameter of AVR's PI controller [28]. The onshore grid voltage (rated voltage 400 kV) decreases by 32 kV at 1 s, it can be observed that: 1) with a larger T_v, the changing rate of voltage at the onshore point of coupling is reduced; 2) the static deviation of voltage is not improved; and 3) the voltage nadir is pulled up and enhanced. This kind of stiffness characteristic provided by the SDViSC is beneficial to improve the voltage dynamics.

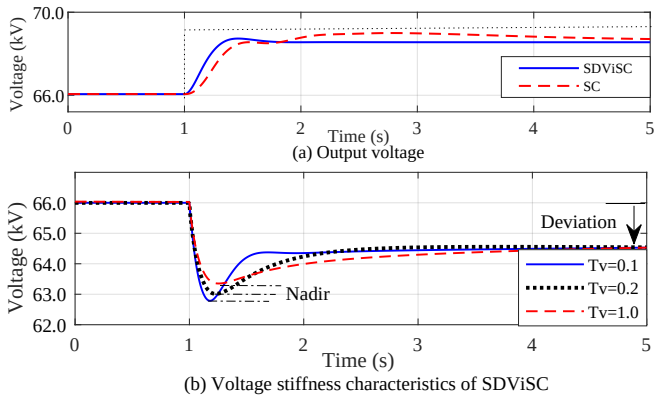

(a) Output voltage

(b) Voltage stiffness characteristics of SDViSC

Fig. 12. Voltage regulation performance and stiffness of SDViSC under a strong onshore grid (SCR=7.14, AVR droop coefficients are both 0.02)

2) Inertia Support: As shown in Fig. 3, the machine side converter is controlled to inject current to the DC link capacitor to maintain a constant voltage during the inertia support process. Therefore, the energy stored in the capacitor (determined by capacitance value) and extracted from the machine side impacts the performance of SDViSC. Here two load-increasing cases are performed:

- i) Load increases by 50 MW: Fig. 13 (a) illustrates the inertia support performance when the SDViSC and traditional SC have the same inertia constant (i.e., H=3s). The system frequency decreases as the load increases and the frequency nadir is almost the same for the SDViSC and SC. Fig. 13 (b) and (c) further present the advantage of the programmability of SDViSC in comparison to SCs. The frequency nadir is decreased when increasing the inertia of SDViSC, which clearly shows its advantage to adapt to the evolution of the grid's needs. The decreased oscillation frequency also indicates enhanced system performance.
- ii) Load increases by 100 MW: Fig. 14 (a) demonstrates the system responses with the SDViSC and traditional SC of the same capacity and inertia constant. It can be seen that the system experiences a larger frequency dip with the SDViSC than that with SC because of the limited stored energy by wind turbines. Fig. 14 (b) presents the frequency responses when paralleling a 2000 Ah Li-ion battery with the DC capacitor. The obviously decreased frequency nadir indicates improved inertia support in comparison with the case having no storage.

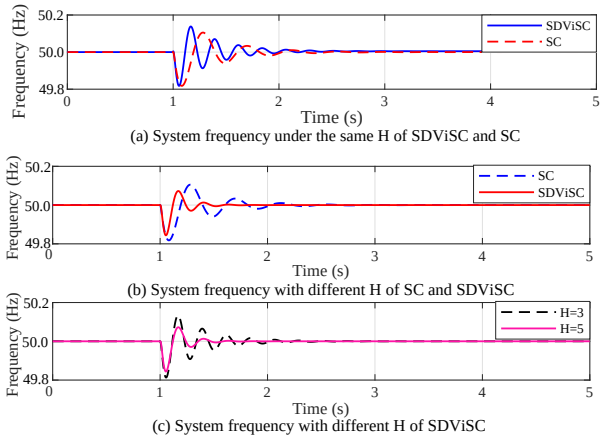

(a) System frequency under the same H of SDViSC and SC

(b) System frequency with different H of SC and SDViSC

(c) System frequency with different H of SDViSC

Fig. 13. System responses with SDViSC and SC under a strong grid (SCR=7.14). (a) with the same H = 3s, (b) with H =3s of SC and H = 5s of SDViSC; (c) Programmable H=3s and H =5s for SDViSC.

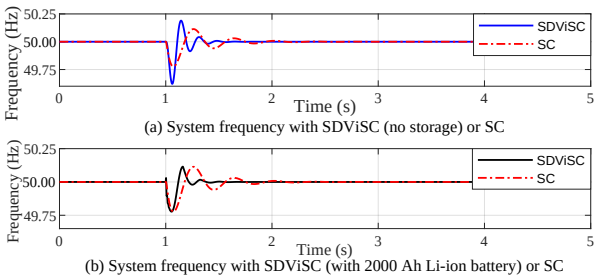

(a) System frequency with SDViSC (no storage) or SC

(b) System frequency with SDViSC (with 2000 Ah Li-ion battery) or SC

Fig. 14. System frequency using SDViSC (without and with storage) and SC with same inertia constant $H = 4$ under a strong grid (SCR=7.14).

As a conclusion, equivalent inertia support as traditional SCs can be offered by the SDViSC when having adequate

stored energy [29]. It is also worth highlighting that the inertia constant of SDViSC can be programmed to satisfy the system's evolving needs. Guaranteeing a solid inertia support service similar to traditional SCs, additional storage equipment is required to be installed or operating multiple WTs as SDViSCs in parallel, which will be validated in subsection IV-E.

3) Short-Circuit Capacity Contribution: The maximum peak current is set to be 0.525 kA (1.5 p.u.) [30]. Fig. 15 presents the outputs of the SDViSC and the traditional SC under a single-phase to ground fault, which starts at 1 s and is cleared at 1.2 s. It can be observed from the results that:

- Both the SDViSC and the traditional SC instantaneously inject reactive power to boost the voltage.
- As shown in Fig. 15 (a), the SC offers a short-circuit current that rises to 1.5 kA (130 MVar) and the residual voltage is above 46 kV.
- The SDViSC's contribution is directly limited by its overcurrent capability, as shown in Fig. 15 (b). The residual voltage is about 38 kV, which is lower than that of the SC. Therefore, an SDViSC with a larger capacity is required to provide comparable short-circuit current as the SC does.

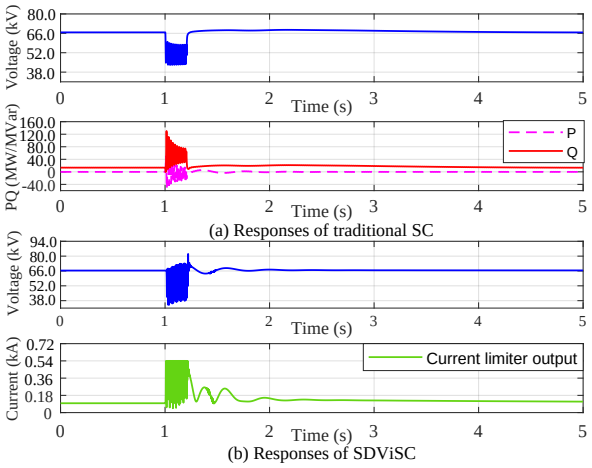

Fig. 15. System responses under grid side faults (SCR=7.14).

4) Grid Strength Enhancement: We compare the capability to suppress instability under weak grid conditions via three cases: 1) without SDViSC or SC, 2) with only SC and 3) with only SDViSC. Fig. 16 presents the results that the studied case is becoming unstable under the largest SCR (the boundary value for system stability and instability). It can be seen that:

- When there is no SC or SDViSC, the system is unstable (see Fig. 16 (a)) when the SCR decreases to 2.04, the voltage oscillates severely and deviates largely from the rated value.
- With SC, the system is stable (see Fig. 16 (b)) under weaker grid conditions (lower SCR) compared with Fig. 16 (a), which shows that the weak grid is indeed enhanced. The system still loses stability when the SCR decreased to 1.58 due to the limited capability of SC.
- With SDViSC, the system can be stabilized under further lower SCR (see Fig. 16 (c)). Thus, the grid-forming control based SDViSC with changeable parameters performs better than SCs to maintain stability under changing conditions.

In summary, the following observations can be obtained:

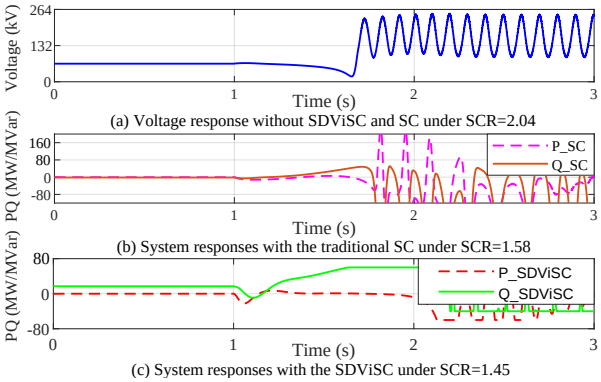

Fig. 16. System responses under weak grids emulated by changing the equivalent impedance (or SCR) of the onshore grid at 1 s.

- The SDViSC outperforms the SC in terms of voltage regulation speed and its voltage stiffness characteristics are beneficial to system voltage dynamics.
- With adequate stored energy, SDViSC can provide equivalent inertia support as the SC, alternative ways are installing extra storage equipment or operating multiple WTs as SDViSCs in parallel to reduce the effects of hardware limitation. Its parameters can be flexibly reconfigured to adapt to changing grid conditions.
- The overcurrent capability of converters, which is definitely below the capability of SC, limits their short-circuit capacity contribution. Quantification for specific converters may be needed before deployment to provide the same contribution.
- The SDViSC with programmable parameters performs better given enough capacity than the SC to maintain transient stability under weak grid conditions.

E. Control Efficacy of SDViSC

We verify SDViSC's control efficacy under three scenarios, including plug-and-play of SDViSCs, parallel operation of SDViSCs and oscillation damping under weak grid conditions.

1) Plug-and-Play of SDViSCs: In this part, we demonstrate how the OWF reacts under the plug-and-play operation of SDViSCs. Specifically, two wind turbines in Cluster 1 and Cluster 4 are plugged into the OWF as SDViSCs at 1.2 s and 4.8 s, respectively. Fig. 17 presents the physical and cyber states of these two SDViSCs before and after the plug operation. It can be observed from the results that:

- When SDViSCs are connected to the OWF, the software-defined controllers immediately start to operate the wind turbines as ViSCs to provide voltage and inertia support.
- As shown in Fig. 17(a)-(d), currents and voltages of SDViSCs can be stabilized in a short time (i.e., within around 0.1s) after the plug operation. This is because the SDViSC retains the fast synchronization property of the traditional synchronous condenser [31], [32]. It indicates a satisfactory transient performance of the designed ViSC control.
- Communication is only required when the wind turbine is operating as a ViSC. Fig. 17 (e) presents the packets received by the two SDViSCs, which clearly show that the SDN controller builds the communication link in a timely manner after receiving a request from the OWFCC.

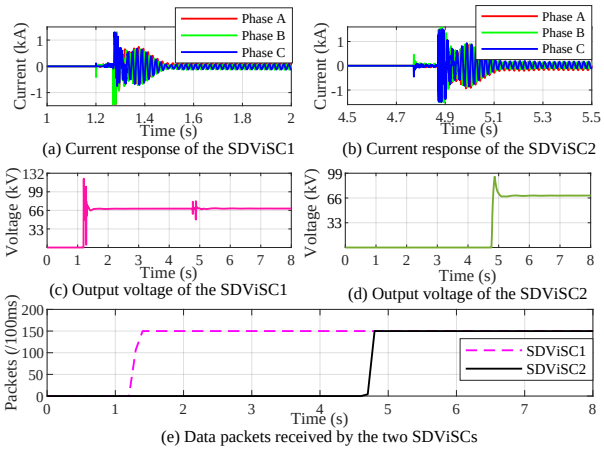

Fig. 17. Physical and cyber states of SDViSCs under plug-and-play.

2) Parallel Operation of SDViSCs for Voltage Regulation: A single SDViSC may not be able to provide the functionalities of a large-capacity SC. Therefore, we propose to operate multiple SDViSCs in parallel to increase the overall capacity.

First, we demonstrate the efficacy of the parallel operation of SDViSCs for providing voltage regulation services. The leftmost 4 wind turbines in Cluster 3 operate in parallel as SDViSCs with voltage droop coefficients of 0.03, 0.05, 0.07, and 0.1. Results are shown in Fig. 18:

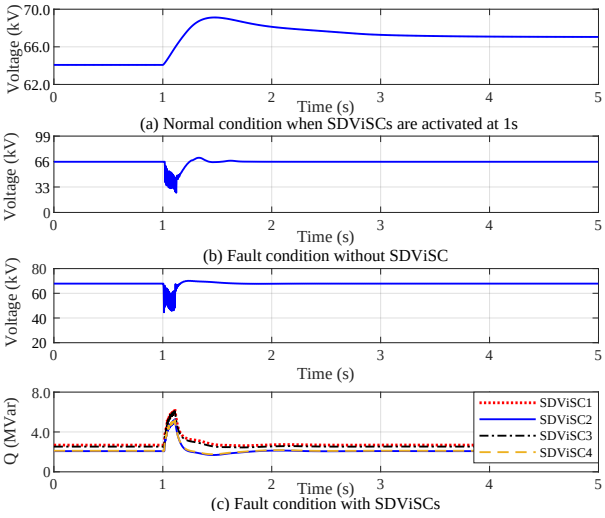

Fig. 18. System responses when in-parallel SDViSCs are activated at 1s.

- Fig. 18 (a) first studies the performance of SDViSCs in normal operating conditions (i.e., without any faults). It can be seen that before the deployment of SDViSC (before 1s), the PCC voltage is 64 kV, which is below the rated voltage. After SDViSCs are activated to inject reactive power, the PCC voltage is accordingly boosted to 67 kV.
- Fig. 18 (b)-(c) further study the system responses under a phase-to-ground fault that occurred at the grid side at 1s. Fig. 18 (b) shows that without SDViSCs, the PCC voltage drops to 27 kV after the fault. However, as shown in Fig. 18 (c), when SDViSCs are deployed, the PCC voltage during and after the fault can be significantly improved. The reason is that SDViSCs perform reactive power sharing according to their voltage droop coefficients to support the grid voltages.

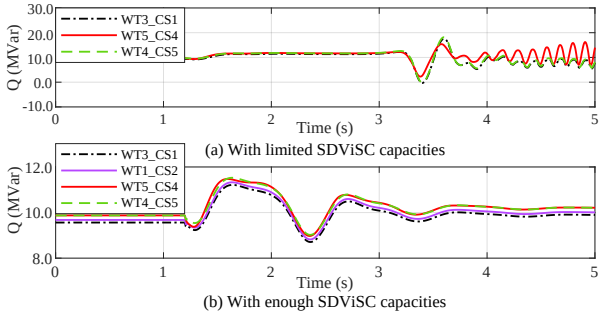

Fig. 19. System response during the transition between strong and weak grid conditions. WT1_CS1: Wind Turbine 1 in Cluster 1.

In summary, simulation results indicate that SDViSCs are competent to provide voltage regulation functionality as traditional SCs under both normal operating and fault conditions.

3) Parallel Operation of SDViSCs for Improving the Transient Stability of Weak Grids: Further, we demonstrate the capability of SDViSCs to improve the system's transient stability under weak grid conditions. At time $t = 1s$, the SCR is changed from 2.5 to 1.51 by adjusting the impedance of the onshore grid to simulate weak grid conditions.

In comparison to the scenario without SDViSCs shown in Fig. 16 (a), Fig. 19 compares the system performance with 3 SDViSCs (i.e., limited ViSC capacities) and 4 SDViSCs (i.e., enough ViSC capacities). It can be observed that:

- With 3 wind turbines operating as SDViSCs, Fig. 19 (a) shows that SDViSCs indeed enhance the system's transient stability compared with Fig. 16 (a), and hence this weak grid can maintain stable until 3s. However, because of the limited capacity of SDViSCs, the system still deviates from the nominal operating point after 3s and finally loses stability.
- Further, with 4 SDViSCs, Fig. 19 (b) shows that the oscillations can be damped and the system can finally achieve a stable operating condition.

In summary, the ability of SDViSCs to improve transient stability can be flexibly programmed by switching the operating modes of wind turbines and changing the number of available ViSC controllers. Therefore, SDViSCs can adaptably satisfy the system needs under changing grid conditions, which outperforms traditional SCs with nonadjustable capacity.

4) Performance of Virtual Friction Control: we show the performance of virtual friction control for oscillation damping under a three-phase short circuit at the grid side. The simulation results without and with activating the virtual friction control are shown in Fig. 20.

As can be seen from the results, there will be oscillations when a fault happens. The frequency deviation is larger and the oscillation decays slowly when the system inertia is small. When the virtual friction control is activated, the frequency deviation is reduced, and the oscillation is suppressed quickly. Therefore, novel control functions can be deployed conveniently to improve the performance of the power grids.

F. Communication Resilience of SDViSC

This subsection demonstrates the communication resilience of the designed SDN-enhanced SDViSC management. Two

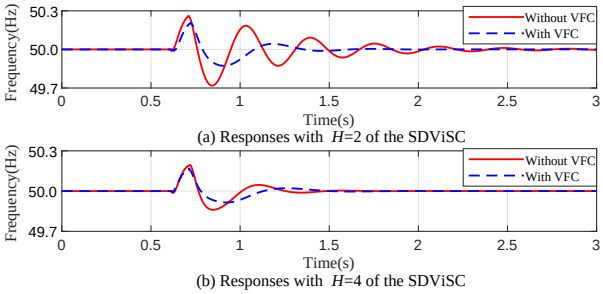

(a) Responses with H=2 of the SDViSC

(b) Responses with H=4 of the SDViSC

Fig. 20. System frequency response without and with activating the virtual friction control (VFC).

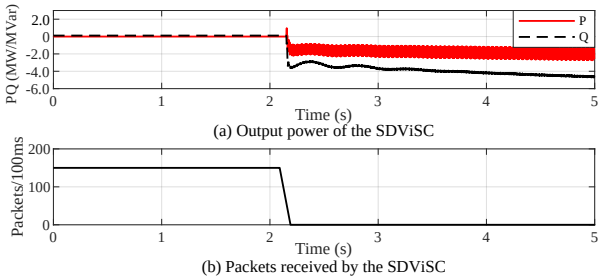

(a) Output power of the SDViSC

(b) Packets received by the SDViSC

Fig. 21. System response without SDN-enabled dynamic routing.

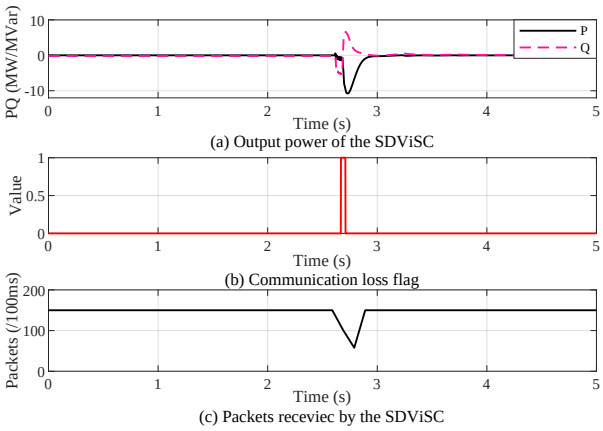

(a) Output power of the SDViSC

(b) Communication loss flag

(c) Packets receviec by the SDViSC

Fig. 22. System response with SDN-enabled dynamic routing.

typical cyber events are studied: 1) communication network impairment and 2) controller failover.

1) Network Impairment: First, we study the performance of SDViSC under network impairments, which may occur frequently in real-world communication networks and can significantly affect the operation of SDViSCs. A physical failure of the communication link of wind turbine 1 in Cluster 1 is triggered to simulate bad network conditions. The testing results without and with the SDN-enabled communication are shown in Figs. 21 and 22, respectively. It can be observed that:

- Without the SDN-based communication scheme, the communication is interrupted immediately when a link fails (see Fig. 21 (b)), and the control signals cannot be transmitted to the SDViSC. Consequently, the SDViSC becomes abnormal without reliable communication (see Fig. 21 (a)).
- With the SDN-based communication scheme, the SDN controller detects a communication loss event (see Fig. 22 (b)), and dynamic routing is performed to switch to another route. Fig. 22 (c) shows that the data transmission quickly recovers. The SDViSC becomes normal after a short transient process.

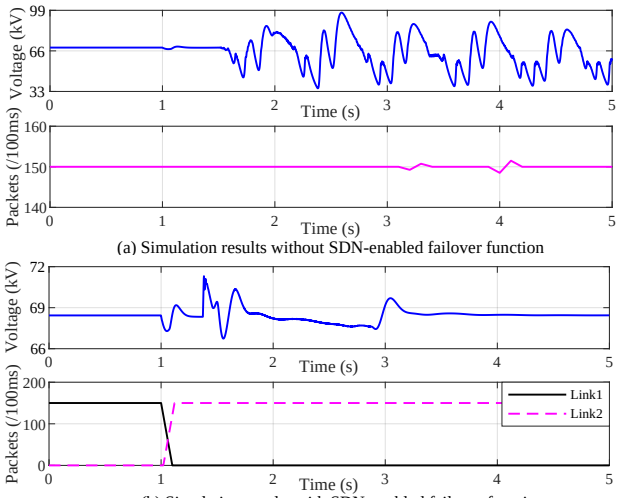

(a) Simulation results without SDN-enabled failover function

(b) Simulation results with SDN-enabled failover function

Fig. 23. SDViSC's response with and without SDN-enabled failover function.

2) Controller Failover: One salient feature of the developed SDN-enhanced SDViSC is the controller failover function, which ensures during any controller failure, a backup controller can be conveniently implemented using software to provide redundancy and reliability for wind farm operations.

Fig. 23 provides the results with and without the SDN-enabled controller failover function carried out for wind turbine 1 in Cluster 1. It can be seen that:

- When the SDN-enabled failover function is disabled, the performance of the SDViSC deteriorates severely after the controller malfunction, even though the cyber network is still working (see Fig. 23 (a)).
- When the failover function is enabled, the backup controller immediately starts to work after the controller malfunction, and the SDN controller establishes a new communication link (see Fig. 23 (b)). The operation of SDViSC becomes normal after a short period of oscillations. The handover capability enabled by the SDN-based communication scheme ensures the stable functioning of SDViSC.

V. Conclusion

In this paper, we devise SDViSC to operate full converter wind turbines as virtual SCs in an unprecedented programmable, adaptable and lightweight manner. A Tustin transformation-based SDC algorithm is developed to virtualize controllers with fast dynamics in SDViSC. An SDN-enabled communication scheme is further established for SDViSC management with great communication resilience and reduced communication burden. A real-time, cyber-in-the-loop prototype for a large wind farm is built to validate the efficacy of SDViSC in an RTDS environment. Extensive experimental results demonstrate that SDViSC can be operated flexibly to provide SC capabilities to support reliable and resilient offshore wind farm operations. Comparison results with SCs show that the hardware limitation can be reduced by using together with storage and enhanced power converters. Protection methods for converters using SDC will be our future research direction.

VI. APPENDIX

A. Wind Turbine Parameters

The parameters of the wind turbine system are provided in Table I.

TABLE I
PARAMETERS OF THE WIND TURBINE SYSTEM

Name	Value	Description
S_{WT}	10 MW	wind turbine rated power
V_l	690 V	grid side converter voltage, line-to-line voltage, rms
C_{dc}	$1.4{\cdot}10^{5}$ μF	DC capacitance
r_f	$2.5133{\cdot}10^{-4}$ Ω	filter resistance
L_f	$1.6000{\cdot}10^{-5}$ H	inverter side filter inductance
r_{cf}	$1.4283{\cdot}10^{-4}$ Ω	filter resistance
c_f	$5.10{\cdot}10^{3}$ μF	filter capacitance
S_T	14 MVA	wind turbine transformer rating
V_m	66 kV	high voltage side, lint-to-line voltage, rms
r_T	1.6425 Ω	transformer resistance (convert to high voltage side)
l_T	0.0517 H	transformer inductance (convert to high voltage side)

The controller parameters are provided in Table II.

TABLE II
CONTROLLER PARAMETERS OF SDVISC

Name	Value	Description
m_q	0.02 p.u.	droop gain of automatic voltage controller
K_{pv}	0.03 p.u.	proportional gain of automatic voltage controller
K_{iv}	0.2 p.u.	integral gain of automatic voltage controller
ω_s	$2\pi \cdot 50$ rad/s	rated angular frequency
H	4s	emulated inertia constant
D	0.5	emulated damping coefficient
R_{vir}	0.2 Ω	virtual resistance
L_{vir}	$6.3662{\cdot}10^{-4}$ H	virtual inductance
K_{pc}	0.2 p.u.	proportional gain of current controller
K_{ic}	5 p.u.	integral gain of current controller
K_{AD}	0.2 p.u.	active damping gain
K_{ffv}	1 p.u.	current controller feedforward gain
K_{pdc}	0.75 p.u.	proportional gain of machine side controller
K_{idc}	0.45 p.u.	integral gain of machine side controller
K_{ppa}	1.4 p.u.	proportional gain pitch angle controller
K_{ipa}	0.2 p.u.	integral gain of pitch angle controller
$\Delta\beta$	5 deg/s	rate limit of pitch angle control
β_{max}	35 deg	angle limit of pitch angle control
T_{LPF}	0.025s	frequency filter time constant
T_{v1}	0.001s	virtual friction controller time constant 1
T_{v2}	0.5s	virtual friction controller time constant 2
K_{F1}	2	virtual friction controller gain 1
K_{F2}	0.6	virtual friction controller gain 2
T_1	3s	lead-lag controller time constant 1
T_2	1.2s	lead-lag controller time constant 2

B. Onshore Grid and Cable Parameters

The parameters of grid side transformers and cables are given in Table III through Table V.

TABLE III
COLLECTION CABLE EQUIVALENT ELECTRICAL PARAMETERS

Rated Voltage	Resistance	Inductance	Capacitance
66 kV	0.06 Ω/km	0.34 mH/km	0.29 μF/km

TABLE IV
TRANSMISSION CABLE EQUIVALENT ELECTRICAL PARAMETERS

Rated power	Resistance	Inductance	Capacitance
220 kV	0.047 Ω/km	0.406 mH/km	0.208 μF/km

TABLE V
GRID SIDE TRANSFORMER ELECTRICAL PARAMETERS

Rated power	Voltage ratio	Short-circuit voltage ($U_k\%$)
550 MVA	400/220	12
Copper loss	Core loss	No load current ($I_0\%$)
700 kW	80 kW	0.1

REFERENCES

[1] "Offshore Wind Power for New York," https://sunrisewindny.com/, 2022.

[2] M. V. Liu and *et al*, "An open source representation for the NYS electric grid to support power grid and market transition studies," *IEEE Trans. Power Syst.*, 2022.

[3] W. Wan, P. Zhang, M. A. Bragin, and P. B. Luh, "Cooperative fault management for resilient integration of renewable energy," *Electr. Power Syst. Res.*, vol. 211, p. 108147, 2022.

[4] H. Wu, X. Wang, and Ł. H. Kocewiak, "Impedance-based stability analysis of voltage-controlled mmcs feeding linear ac systems," *IEEE J. Emerg. Sel. Top. Power Electron.*, vol. 8, no. 4, pp. 4060–4074, 2019.

[5] M. K. Bakhshizadeh and *et al*, "Improving the impedance-based stability criterion by using the vector fitting method," *IEEE Trans. Energy Convers.*, vol. 33, no. 4, pp. 1739–1747, 2018.

[6] C. Li, S. Wang, F. Colas, and J. Liang, "Dominant instability mechanism of vsi connecting to a very weak grid," *IEEE Trans. Power Syst.*, vol. 37, no. 1, pp. 828–831, 2022.

[7] H. T. Nguyen, G. Yang, A. H. Nielsen, and P. H. Jensen, "Combination of synchronous condenser and synthetic inertia for frequency stability enhancement in low-inertia systems," *IEEE Trans. Sustain. Energy.*, vol. 10, no. 3, pp. 997–1005, 2019.

[8] H. T. Nguyen and *et al*, "Applying synchronous condenser for damping provision in converter-dominated power system," *J. Modern Power Syst. Clean Ener.*, vol. 9, no. 3, pp. 639–647, 2020.

[9] J. Jia and *et al*, "Impact of VSC control strategies and incorporation of synchronous condensers on distance protection under unbalanced faults," *IEEE Trans. Ind. Electron.*, vol. 66, no. 2, pp. 1108–1118, 2018.

[10] Y. Wang, L. Wang, and Q. Jiang, "Impact of synchronous condenser on sub/super-synchronous oscillations in wind farms," *IEEE Trans. Power Deliv.*, vol. 36, no. 4, pp. 2075–2084, 2020.

[11] H. T. Nguyen, M. N. Chleirigh, and G. Yang, "A technical & economic evaluation of inertial response from wind generators and synchronous condensers," *IEEE Access*, vol. 9, pp. 7183–7192, 2021.

[12] L. Bao and *et al*, "Wind farms in weak grids stability enhancement: SynCon or STATCOM?" *Electr. Power Syst. Res.*, vol. 202, 2022.

[13] Q.-C. Zhong and G. Weiss, "Synchronverters: Inverters that mimic synchronous generators," *IEEE Trans. Indust. Electron.*, vol. 58, no. 4, pp. 1259–1267, 2011.

[14] Q.-C. Zhong, G. C. Konstantopoulos, B. Ren, and M. Krstic, "Improved synchronverters with bounded frequency and voltage for smart grid integration," *IEEE Transactions on Smart Grid*, vol. 9, no. 2, pp. 786–796, 2018.

[15] K. Jiang, H. Su, H. Lin, K. He, H. Zeng, and Y. Che, "A practical secondary frequency control strategy for virtual synchronous generator," *IEEE Transactions on Smart Grid*, vol. 11, no. 3, pp. 2734–2736, 2020.

[16] L. Kocewiak and *et al*, "Overview status and outline of stability analysis in converter-based power systems," in *Proc. Virtual Wind Integr. Workshop*, 2020, p. 10.

[17] L. Wang, Y. Qin, Z. Tang, and P. Zhang, "Software-defined microgrid control: The genesis of decoupled cyber-physical microgrids," *IEEE Open Access J. power energy*, vol. 7, pp. 173–182, 2020.

[18] O. Mo, S. D'Arco, and J. A. Suul, "Evaluation of virtual synchronous machines with dynamic or quasi-stationary machine models," *IEEE Trans. Industr. Electron.*, vol. 64, no. 7, pp. 5952–5962, 2017.

[19] M. G. Taul and *et al*, "Current limiting control with enhanced dynamics of grid-forming converters during fault conditions," *IEEE J. Emerg. Sel. Top. Power Electron.*, vol. 8, no. 2, pp. 1062–1073, 2019.

[20] M. Chinchilla and *et al*, "Control of permanent-magnet generators applied to variable-speed wind-energy systems connected to the grid," *IEEE Trans. Energy Convers.*, vol. 21, no. 1, pp. 130–135, 2006.
[21] X. Lyu, J. Zhao, Y. Jia, Z. Xu, and K. P. Wong, "Coordinated control strategies of PMSG-based wind turbine for smoothing power fluctuations," *IEEE Trans. Power Syst.*, vol. 34, no. 1, pp. 391–401, 2019.
[22] R. Zhao and *et al*, "A novel discretization method for multiple second-order generalized integrators," *IEEE Trans. Power Electron.*, vol. 36, no. 10, pp. 10 998–11 002, 2021.
[23] M. Al-Alaoui, "Novel approach to analog-to-digital transforms," *IEEE Trans. Circuits Syst. I: Regul. Pap.*, vol. 54, no. 2, pp. 338–350, 2007.
[24] P. Zhang, B. Wang, P. B. Luh, L. Ren, and Y. Qin, "Enabling resilient microgrid through ultra-fast programmable network," Dec. 10, 2019, US Patent 10,505,853.
[25] P. Zhang, *Networked microgrids*. Cambridge University Press, 2021.
[26] Y. Qi, H. Zhao, S. Fan, A. M. Gole, H. Ding, and I. T. Fernando, "Small signal frequency-domain model of a lcc-hvdc converter based on an infinite series-converter approach," *IEEE Transactions on Power Delivery*, vol. 34, no. 1, pp. 95–106, 2019.
[27] S. Jiang and G. Konstantinou, "Impedance-based stability analysis: Nodal admittance or bus admittance?" *IEEE Transactions on Power Systems*, vol. 39, no. 1, pp. 2327–2340, 2024.
[28] L. Shang and *et al*, "VSC–based voltage stiffness compensator to improve grid voltage dynamics," *Front. Energy Res.*, p. 3, 2022.
[29] T. Ding and *et al*, "Two-stage chance-constrained stochastic thermal unit commitment for optimal provision of virtual inertia in wind-storage systems," *IEEE Trans. Power Syst.*, vol. 36, no. 4, pp. 3520–3530, 2021.
[30] D. Lepour and *et al*, "Performance assessment of synchronous condensers vs voltage source converters providing grid-forming functions," in *2021 IEEE Madrid PowerTech*. IEEE, 2021, pp. 1–6.
[31] M. Schweizer, S. Almér, S. Pettersson, A. Merkert, V. Bergemann, and L. Harnefors, "Grid-forming vector current control," *IEEE Transactions on Power Electronics*, vol. 37, no. 11, pp. 13 091–13 106, 2022.
[32] O. Stanojev, U. Markovic, P. Aristidou, and G. Hug, "Improving stability of low-inertia systems using virtual induction machine synchronization for grid-following converters," *IEEE Transactions on Power Systems*, vol. 38, no. 3, pp. 2290–2303, 2023.

Zimin Jiang (Graduate Student Member, IEEE) received the B.S. degree in electrical engineering from Shandong University, Jinan, China, in 2015. He is currently pursuing the Ph.D. degree in electrical engineering with Stony Brook University, Stony Brook, NY, USA. His current research interests include power system stability and control, microgrids, cyber-physical security, offshore wind integration, and AI-enabled control algorithms in power systems.

Peng Zhang received the Ph.D. degree in electrical engineering from the University of British Columbia, Vancouver, BC, Canada, in 2009. He is a Full Professor of Electrical and Computer Engineering, and a SUNY Empire Innovation Professor at Stony Brook University, New York. Previously, he was a Centennial Associate Professor and a Francis L. Castleman Associate Professor at the University of Connecticut, Storrs, CT, USA. He was a System Planning Engineer at BC Hydro and Power Authority, Canada, during 2006-2010. His research interests include AI-enabled smart grids, quantum-engineered power grids, networked microgrids, power system stability and control, cybersecurity, and formal methods and reachability analysis.

Dr. Zhang is an individual member of CIGRÉ. He serves as the Founding Editor for the IEEE Press Series on Offshore Wind Energy Collection. He was a 2024 Outstanding Associate Editor for the IEEE Transactions on Power Systems.

Yifan Zhou (Member, IEEE) received the B.S. and Ph.D. degrees in electrical engineering from Tsinghua University, Beijing, China, in 2014 and 2019, respectively. She has been a Postdoctoral Researcher with Stony Brook University, Stony Brook, NY, USA. She is currently an Assistant Professor with Stony Brook University. Her research interests include microgrid stability and control, formal methods, reachability analysis, and quantum computing.

Lukasz Kocewiak (Senior Member, IEEE) received the B.S. and M.S. degrees in electrical engineering from the Warsaw University of Technology, Warsaw, Poland, in 2007, and the Ph.D. degree from Aalborg University, Aalborg, Denmark, in 2012. He is currently with Ørsted and is working as a Digital Product Manager. He is a Power System Specialist within the area of design of electrical infrastructure in large offshore wind power plants. He is the author and co-author of more than 100 publications. His research interests include harmonics, stability and nonlinear dynamics in power electronics and power systems especially focused on wind power generation units. He is a member of various working groups and activities within CIGRÉ and IEC.

Divya Kurthakoti Chandrashekhara received the M.S. and Ph.D. degrees in electrical engineering from Indian Institute of Science, Bangalore, India, in 2002 and 2006, respectively. She is currently with Ørsted and is working as a Senior Lead Specialist.

Marie-Lou Picherit received the Ph.D. degree in environmental sciences and engineering from École Nationale Supérieure des Mines de Saint-Étienne, France, in 2010. She is currently with Ørsted and is working as a Product Program Manager.

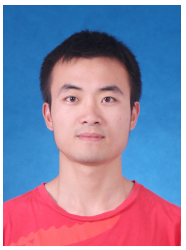

Zefan Tang (Member, IEEE) is currently a Senior Data Scientist at Eversource Energy. He earned his B.S. degree from Zhejiang University, M.S. from Shanghai Jiao Tong University, and Ph.D. from Stony Brook University in 2014, 2017, and 2021, respectively. Prior to joining Eversource, Dr. Tang held a postdoctoral researcher position at Brookhaven National Laboratory from 2021 to 2022. His research interests include microgrids, quantum security, quantum computing, artificial intelligence, software-defined networking, and cyber-physical security.

Kenneth B. Bowes received the B.Sc. degree in electrical engineering from the University of New Hampshire, Durham, NH, USA, and the M.Sc. degree in electrical engineering from the Rensselaer Polytechnic Institute, Troy, NY, USA.

He is the Vice President of Transmission Performance with Eversource Energy, Berlin, CT, USA. In that role, he is responsible for the leadership and direction of transmission performance as it relates to short- and long-term customer impacts and benefits, development of key siting witnesses, transmission performance indicators, Federal Energy Regulatory Commission and State Regulatory plans, and operational compliance. He serves as a technical consultant and expert witness for various regulatory proceedings and large transmission projects including Northern Pass Transmission and Bay State Wind. He has been part of the Eversource team for over 30 years, beginning in the System Test department. Since that time, he has held a variety of positions with increasing responsibility in the Engineering and Transmission areas, most recently serving as the Vice President of Engineering for Eversources Connecticut Operations. In that previous role, he was responsible for all engineering activities for the electric distribution systems including distribution planning, distribution engineering and design, substation engineering, protection and control engineering, telecommunications engineering, and the geographic information systems for electric and gas operations. He established the reliability, asset management, and system resiliency strategies for a $ 300 million annual program development and five-year capital program. He also managed the distributed generation, microgrid, new technology, and R&D activities for the company. Additionally, he executed the five-year $ 450 million System Resiliency Program and the Stamford and Greenwich Infrastructure Improvement Projects. Under his leadership, Eversource received both the Emergency Recovery Award and the Emergency Assistance Award from the Edison Electric Institute in 2013.

Mr. Bowes is the past Chairman of the Edison Electric Institute's Transmission Committee and presently serves on the EEI Transmission and EEI Security Committees. He serves on the Board of Directors of Special Olympics Connecticut and the Bristol Boys and Girls Club. He is the Chairman of the Board of Nutmeg Big Brothers Big Sisters.

Guangya Yang (Senior Member, IEEE) received his PhD in 2008 and subsequently joined the Technical University of Denmark. From 2020 to 2021, he was a full-time Specialist in electrical design, control, and protection of large offshore wind farms with Ørsted. He is currently an Associate Professor at the Technical University of Denmark. His research interests include the stability and protection of converter-based power systems, with an emphasis on offshore wind applications, as well as the cyber-physical security of power systems. He is the Convener of IEC61400-21-5 on configuration, functional specification, and validation of hardware-in-the-loop test bench for wind power plants. In addition, he serves as the Coordinator of the H2020 Marie Curie Innovative Training Network Project Innovative Tools for Cyber-Physical Energy Systems (InnoCyPES) and as the Lead Editor of the Power and Energy Society Section in IEEE Access.